Cracking pre-40S ribosomal subunit structure by systematic analyses of RNA-protein cross-linking

The EMBO Journal (2010) 29, 2026–2036 | © 2010 European Molecular Biology Organization | Some Rights Reserved 0261-4189/10
www.embojournal.org

THE EMBO JOURNAL

EMBO open

Cracking pre-40S ribosomal subunit structure by systematic analyses of RNA–protein cross-linking

Sander Granneman, Elisabeth Petfalski, Agata Swiatkowska and David Tollervey*

Wellcome Trust Centre for Cell Biology, University of Edinburgh, Edinburgh, Scotland, UK

Understanding of eukaryotic ribosome synthesis has been slowed by a lack of structural data for the pre-ribosomal particles. We report rRNA-binding sites for six late-acting 40S ribosome synthesis factors, three of which cluster around the 3′ end of the 18S rRNA in model 3D structures. Enp1 and Ltv1 were previously implicated in 'beak' structure formation during 40S maturation—and their binding sites indicate direct functions. The kinase Rio2, putative GTPase Tsr1 and dimethylase Dim1 bind sequences involved in tRNA interactions and mRNA decoding, indicating that their presence is incompatible with translation. The Dim1- and Tsr1-binding sites overlap with those of homologous *Escherichia coli* proteins, revealing conservation in assembly pathways. The primary binding sites for the 18S 3′-endonuclease Nob1 are distinct from its cleavage site and were unaltered by mutation of the catalytic PIN domain. Structure probing indicated that at steady state the cleavage site is likely unbound by Nob1 and flexible in the pre-rRNA. Nob1 binds before pre-rRNA cleavage, and we conclude that structural reorganization is needed to bring together the catalytic PIN domain and its target.

The EMBO Journal (2010) **29,** 2026–2036. doi:10.1038/emboj.2010.86; Published online 7 May 2010
Subject Categories: RNA; structural biology
Keywords: CRAC; pre-ribosome; ribosome synthesis; RNP structure; yeast

Introduction

Biogenesis of the mature 40S and 60S ribosomal subunits is an exceptionally complex process in eukaryotes, which requires the activities of roughly 200 synthesis factors for rRNA maturation and subunit assembly (reviewed in Henras *et al*, 2008). In the nucleolus, RNA polymerase I generates a polycistronic precursor rRNA (35S pre-RNA) that contains the sequences for the mature 18S, 5.8S and 25S rRNA, flanked by the external transcribed spacers (5′-ETS and 3′-ETS) and separated by the internal transcribed spacers (ITS1 and ITS2; Supplementary Figure 1). The 35S pre-rRNA is cleaved at processing sites A_0, A_1 and A_2, within a large, ~90S complex, to yield a pre-40S particle that contains the 20S pre-rRNA and a pre-60S particle containing the $27SA_2$ pre-rRNA. The pre-60S particles undergo a complex maturation pathway in the nucleolus, nucleoplasm and cytoplasm (reviewed in Henras *et al*, 2008). In contrast, the pre-40S particles are rapidly exported to the cytoplasm. Here, the 20S pre-rRNA is modified close to the 3′ end of the 18S rRNA sequence by the dimethylase Dim1 (Lafontaine *et al*, 1994), before cleavage by the PIN-domain endonuclease Nob1 to generate the mature 18S rRNA (Pertschy *et al*, 2009) (Supplementary Figure 1). Notably, both Dim1 and Nob1 bind the nuclear 90S pre-ribosomes and are exported to the cytoplasm together with the pre-40S particles (Schafer *et al*, 2003). This implies a mechanism that inhibits the premature activity of these enzymes on the substrates with which they are associated, possibly involving structural reorganization of the pre-40S particles. Dim1 is essential for viability, but its essential function is not 18S rRNA methylation, but pre-rRNA cleavage at sites A_1 and A_2 (Lafontaine *et al*, 1995). The basis of this requirement was, however, unclear. Structural reorganization of the pre-40S particle does occur, most notably in formation of the beak structure; a prominent feature of the mature subunit that is absent from pre-40S particles (Schafer *et al*, 2006). This reorganization involves phosphorylation of Enp1 and Ltv1 by the kinase Hrr25, and subsequent dephosphorylation of Rps3 but the roles of Enp1 and Ltv1 in this process were unclear. Late pre-40S particles contain a different protein kinase, Rio2, the targets for which are unknown, and a putative GTPase, Tsr1. Both are needed for 20S–18S processing but, again, their actual roles are unclear.

Affinity purification and mass spectrometry allowed the composition of many pre-ribosomal complexes to be determined, whereas genetic analyses showed that loss of ribosome synthesis factors impeded pre-rRNA processing at specific stages (see Fromont-Racine *et al*, 2003; Henras *et al*, 2008). However, in few cases it was clear how these factors actually participated in pre-rRNA processing. Numerous sub-complexes and other protein–protein interactions between ribosome synthesis factors have been identified (reviewed in Henras *et al*, 2008; Tarassov *et al*, 2008) but little is known about the architecture and structure of these RNP complexes. EM structural analyses of pre-ribosomes have given important insights (Nissan *et al*, 2004; Schafer *et al*, 2006; Ulbrich *et al*, 2009) but these studies are technically challenging, due in part to instability and heterogeneity of purified particles.

The most informative single piece of data that could be provided (short of actual crystal structures of pre-ribosomes) would be the locations of the binding sites for the proteins on

*Corresponding author. Wellcome Trust Centre for Cell Biology and Centre for Systems Biology at Edinburgh, University of Edinburgh, Michael Swann Building, King's Buildings, Mayfield Road, Edinburgh EH9 3JR, Scotland, UK. Tel.: +44 131 650 7092; Fax: +44 131 650 7040; E-mail: d.tollervey@ed.ac.uk

Received: 30 November 2009; accepted: 14 April 2010; published online: 7 May 2010

the pre-rRNAs. This information would be of key importance in establishing a detailed blueprint for ribosome assembly and lend focus to all future characterization of these proteins. With the aim of generating a map of protein–RNA interactions within pre-ribosomes, we performed a systematic UV cross-linking and cDNA analysis (CRAC) (Granneman *et al*, 2009) as outlined in Supplementary Figure 2.

The best characterized, and simplest, pre-ribosomes are the late pre-40S particles. Here, we report the rRNA-binding sites for six factors that are retained in late pre-40S subunits. The findings provide insights into the 40S ribosome synthesis pathway and offer many avenues for future analyses.

Results

UV cross-linking of pre-40S-associated proteins

We tested eight factors known to associate with late pre-40S complexes; Dim1, Dim2/Pno1, Enp1, Ltv1, Nob1, Rio1/Rrp10, Rio2 and Tsr1 and identified binding sites for all except Dim2 and Rio1 (see Supplementary Table 1 for references). Rio1 was poorly cross-linked, whereas Dim2 was cross-linked but numerous attempts failed to reproducibly identify a clear RNA target sequence (data not shown). None of the C-terminal HTP fusions detectably impaired cell growth (Supplementary Figure 3A). Pre-rRNA processing was also unaffected in all strains except Nob1-HTP, which conferred a mild 20S-processing defect (Supplementary Figure 3B). HTP-tagging Nob1 at the N-terminus did not noticeably affect Nob1 function (Supplementary Figure 4C). CRAC experiments were performed 2–5 times, and we monitored the enrichment of tagged proteins in TEV and nickel eluates by western blot analysis (data not shown). To be considered a *bona fide* RNA-binding site, a nucleotide sequence had to be significantly enriched in every experiment.

The locations of identified cross-linked RNA sequences are plotted in Figure 1. Sanger sequences of 50–80 cDNA clones obtained from independent experiments were aligned to a yeast non-coding RNA database using both Blast and Novoalign to align the fragments to the reference sequences and Novoalign was used to locate mutations and calculate percentage of mutations (see Materials and methods). The locations of the hits obtained for each protein using Novoalign are shown aligned against the 18S rRNA sequence, annotated with the predicted secondary structure, in Supplementary Tables 4–9. Cross-linking sites were precisely identified by the presence of multiple point deletions or substitutions at a specific position in sequence reads, or a minimal RNA-binding site was determined from overlapping sequences. Except for Tsr1 and Dim1 (see below), there was little overlap between major peaks in the histograms for each protein, showing that these peaks represent unique RNA-binding sites. Figure 1B shows the results of three independent CRAC experiments performed with an untagged strain, which served as a negative control. The most abundant contaminants (asterisks in Figure 1; Supplementary Figure 3B) were derived from regions near the 3′ end of the 25S rRNA (position ~5800 in rDNA). These were almost always observed in CRAC experiments (Granneman *et al*, 2009), but generally represented a larger fraction of the sequences recovered with proteins that cross-linked less efficiently to RNA.

Enp1 and Ltv1 bind the rRNA near the beak structure

A major structural rearrangement in pre-40S complexes is the formation of the characteristic 'beak' structure, which is shaped by protrusion of helix 33 (H33). Cryo-EM and biochemical studies revealed that beak formation requires a cascade of phosphorylation and dephosphorylation events in the cytoplasm, leading to the stable association of Rps3 and release of assembly factors Ltv1 and Enp1 (Schafer *et al*, 2006). Premature formation of the rigid beak structure is likely to hinder nuclear export of pre-40S complexes, as complexes lacking Ltv1 or Hrr25, the kinase responsible for Enp1, Rps3 and Ltv1 phosphorylation, are not efficiently exported to the cytoplasm (Schafer *et al*, 2006; Seiser *et al*, 2006). Regulation of the timing of beak structure formation is therefore important.

Among all Enp1-associated sequence reads mapped to the rDNA, 64% included the sequence of H33 (Figure 1A; Supplementary Table 5). Deletions and point mutations were found in the internal loop of H33 (nt 1256–1259), pinpointing a cross-linking site (Figure 2B) and positioning Enp1 directly in the beak. Cross-linking to the adjacent H34 was observed less frequently (Figures 1A and 2B). Cryo-EM reconstruction images indicated that in pre-40S particles H33 was flipped sideways (Schafer *et al*, 2006) and it seems probable that this correlates with the binding of Enp1 to H33.

Most RNAs cross-linked to Ltv1 mapped to H16 and H41/41A (Figures 1A and 2B; Supplementary Table 6). Mutations identified in the terminal loop of H16 and in a bulge near H41A reveal the precise cross-linking sites (Figure 2B, nt 453–454, 1490–1491). Cross-links to H21, H39 and H40 were found less frequently (Figure 1A).

In the yeast 40S structure model (Figure 3A), H41A is located in close proximity to the beak and to Rps3, consistent with two-hybrid interactions reported between Rps3 and Ltv1 (Ito *et al*, 2001), whereas H16 is more distantly located in the shoulder region. Simultaneous binding of Ltv1 to both H16 and H41A would require that Ltv1 span the gap between the head and the shoulder (Figure 3C). Although we cannot exclude the possibility that these sites are not occupied simultaneously, it is notable that the cryo-EM structure does indeed show appropriate density to correspond to Ltv1 bound across this region (Figure 3B) (see Discussion).

Collectively, these CRAC results are in good agreement with previously published biochemical and genetic data, and support the model that release of Enp1 and Ltv1 is directly linked to beak structure formation (see Figure 3C).

Rio2 binds the 18S rRNA at the mRNA tunnel in pre-40S complexes

Rio1 and Rio2 are serine kinases involved in processing of 20S pre-rRNA in the cytoplasm. Rio2, but not Rio1, is stably associated with pre-40S complexes (Vanrobays *et al*, 2003), probably explaining why only Rio2 was detectably cross-linked to pre-rRNA (Supplementary Table 1). Rio2 preferentially cross-linked to a terminal loop in H31 (nt 1194–1196) (Figures 1A and 2B; Supplementary Table 8). Loss of modification of residue U1191 in the H31 loop was recently reported to inhibit site D cleavage (Liang *et al*, 2009), suggesting that this may influence the binding or activity of Rio2.

H31 is located in the head of the mature 40S subunit, in a region also likely occupied by Rps15, Rps16, Rps18, Rps20

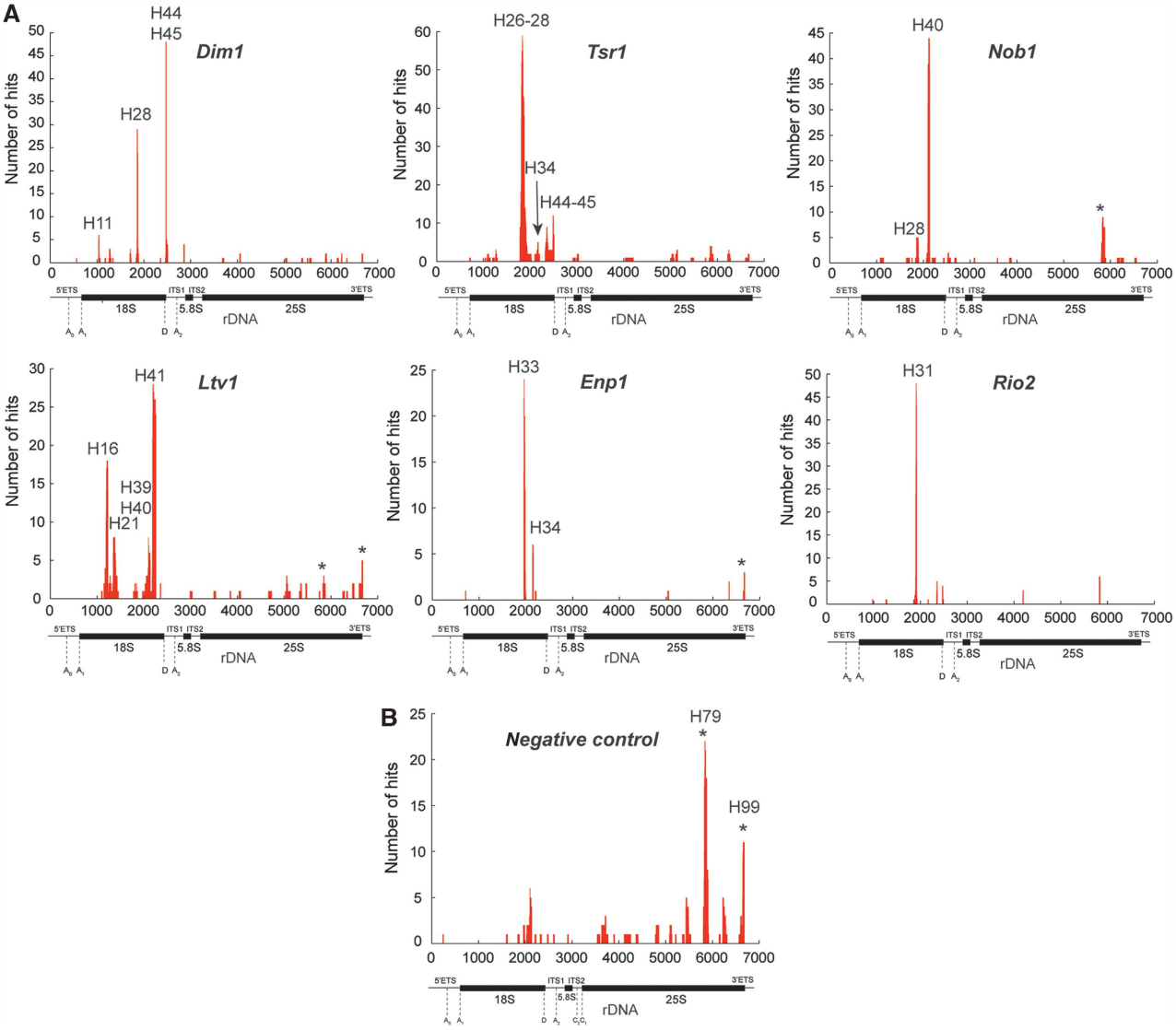

Figure 1 Overview of CRAC results. Shown are the results from independent CRAC experiments performed on pre-40S-associated proteins (**A**). Results from untagged strains are shown in (**B**). Sequences were aligned to the rDNA reference sequence using blast and plotted using gnuplot. The locations of mature rRNA sequences, spacers and cleavage site are indicated below the *x* axis. The *y* axis shows the total number of times each nucleotide within an RNA fragment was mapped to the rDNA sequence. The location of the peaks in the secondary structure of the rRNA (see Figure 2A, B) is indicated with helix (H) numbers. The asterisks indicate frequent contaminants.

and Rps29 (Figures 2B and 3D) (Spahn *et al*, 2001; Brodersen *et al*, 2002). The Rio2 cross-linking sites are located in the cleft that, in the 80S ribosome, is occupied by the P-site tRNA and the C-terminal domains of Rps16 and Rps18 (Spahn *et al*, 2001). This makes it very likely that the association of Rio2 with the pre-40S particles is incompatible with tRNA binding.

Dim1 and the putative GTP-binding protein Tsr1 interact with the central pseudoknot and the decoding centre

Dim1 dimethylates two adenosines in the loop of H45 (indicated as '-m' in Figure 2B) (Lafontaine *et al*, 1994) and the methylation sites were recovered in several sequence reads. However, a major Dim1 cross-linking site was located in the adjacent H44 region (nt 1753–1794) (Figures 1 and 2B; Supplementary Table 4). A second major peak covered sequences over H2 and the adjacent H28 region (nt 1137–1156). H2 base pairs with the 5′ end of 18S rRNA to form the central pseudoknot. Strains lacking Dim1 are unable to cleave site A_1 at the 5′ end of 18S rRNA (Lafontaine *et al*, 1995), and we predict this requirement reflects its interaction with the central pseudoknot. H28 is required for recruitment of the initiator methionine tRNA (Dong *et al*, 2008) and Dim1 binding here would be incompatible with $tRNA^{iMet}$ association. Cross-linking to H11, near the Rps11-binding site (Dresios *et al*, 2005), was also reproducibly observed but with fewer hits (Figures 1A, 2B and 3E).

Tsr1 is required for cleavage of the 20S pre-rRNA at site D to generate 18S rRNA (Gelperin *et al*, 2001) and has a region related to the GTPase domain of elongation factor Tu, although GTP binding and hydrolysis have not yet been reported. The major binding site for Tsr1 was located in the central domain of the 18S rRNA over H19 and H26–29 (Figures 1A and 2B; Supplementary Table 9). These sequences form a large domain within the platform and neck regions of 40S subunits (Spahn *et al*, 2001) (Figure 2B). The average read-length for H19–H26–29 sequences associated

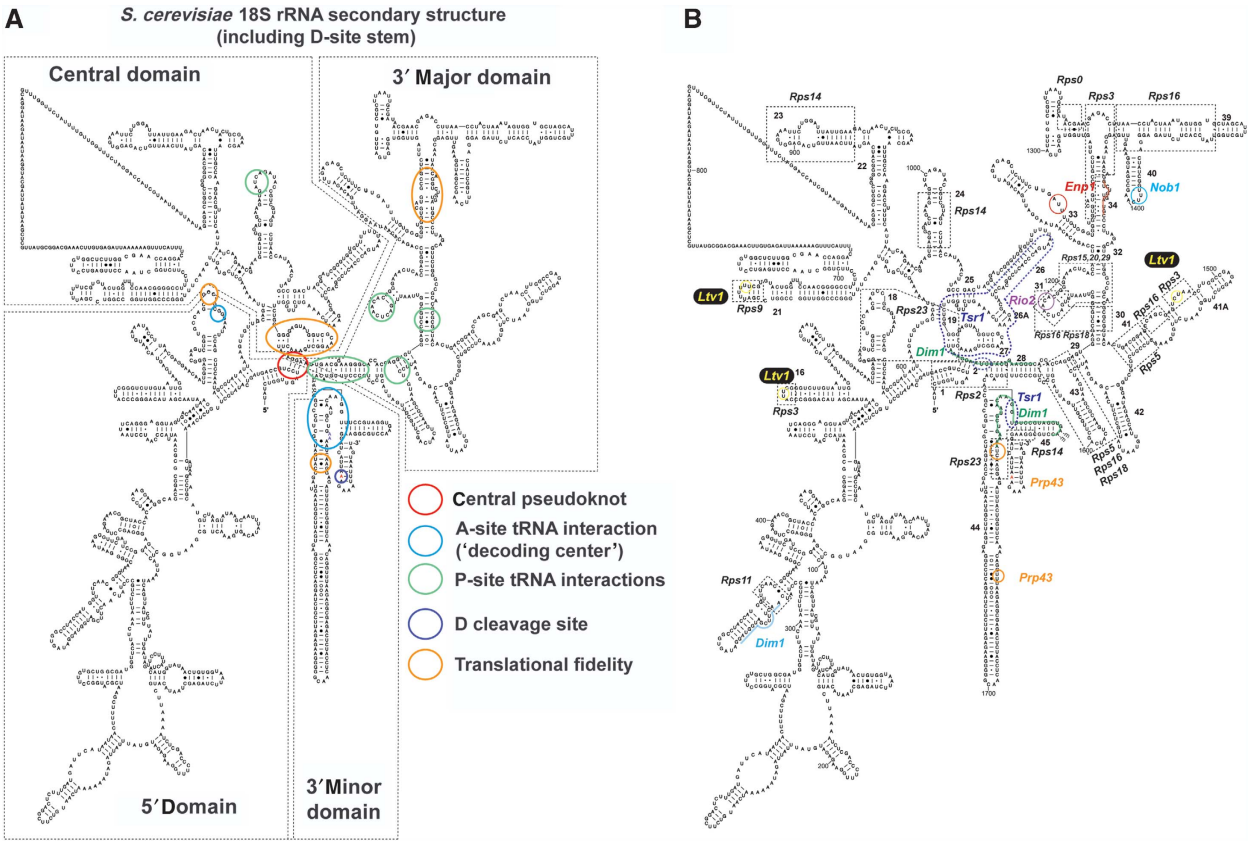

Figure 2 Locations of protein–RNA interaction sites in the 18S rRNA secondary structure. (**A**) Overview of the yeast 18S rRNA secondary structure (obtained from http://www.rna.ccbb.utexas.edu/). The stem including the D-cleavage site was added separately. The 18S rRNA domains are indicated as dashed boxes. Functionally, important elements (central pseudoknot, decoding centre, P-site tRNA interactions, D-cleavage site (coloured red)) are marked with circles. (**B**) Overview of RNA-binding sites for pre-40S-associated proteins. Specific nucleotides cross-linked to proteins are indicated as coloured circles. For cases where no or few mutations were found in cross-linked RNAs (Tsr1 H26 and H27, Dim1 H28 and the Enp1-binding site in H34), the binding sites are indicated by dashed lines. Dashed boxes indicate predicted ribosomal protein (Rps) interaction sites on the 18S rRNA, based on the locations of homologous *T. thermophilus* ribosomal proteins in the 30S crystal structure, the yeast 40S structure model and various other studies performed on ribosomal proteins in yeast (Spahn *et al*, 2001; Brodersen *et al*, 2002; Antunez de Mayolo and Woolford, 2003; Dresios *et al*, 2005). Helix numbering was adopted from Brodersen *et al* (2002). RNA-binding sites for the RNA helicase Prp43 (Bohnsack *et al*, 2009) are also included.

with Tsr1 was 41 nt, against an overall average of 28 nt for other pre-40S proteins. This indicates that this region is relatively resistant to RNase digestion, suggesting a stable structure. Shorter fragments were also identified in helices 26, 27 and in the region spanning helices 2 and 28, with the latter overlapping the Dim1-binding site (Figure 2B). Among the Tsr1 reads derived from the H28 region, 25% contained mutations in a single-stranded sequence located between H2 and H28 (nt 1143–1146), precisely defining the Tsr1-binding site in this region. Notably, these mutations were not found in the Dim1-binding site in the H28 region (Supplementary Table 4).

Twenty five per cent of Tsr1 hits mapped to the 3′ minor domain of 18S rRNA, in H44 and H45 (Figure 1A), close to the cleavage site at the 3′ end of the 18S rRNA (site D) and partially overlapping the major Dim1-binding site (Figure 2A and B). Among the H45 hits, 44% contained mutations (nt 1765–1771, Figure 2B), identifying the direct binding site. Tsr1 binding near site D is consistent with a proposed direct role in 18S rRNA processing (Gelperin *et al*, 2001).

In the crystal structure of the 30S *Thermus thermophilus* ribosomal subunit, H26 and H27 loop around H45 in the vicinity of the 3′ end of the 16S rRNA (see Figure 3E). In addition, the hairpin loop of H27 makes extensive minor groove contacts with H44 just below the decoding centre (see Figure 3E) (Clemons *et al*, 1999; Voorhees *et al*, 2009). Tsr1 could therefore bind simultaneously with the H27–28 and H44–45 regions.

A lower frequency of Tsr1 cross-linking was recovered with H34 (Figure 1A), close to the Rps5-binding site in regions involved in P-site tRNA interactions (Figure 2A) (Spahn *et al*, 2001). The Tsr1 hits in this region are not the same as the negative control, indicating that this interaction is specific.

We conclude that both Dim1 and Tsr1 bind to sequences in the 18S rRNA that includes the decoding centre and regions required for tRNA association with the ribosome. These binding sites are incompatible with the formation of a translation initiation complex. For example, the Dim1-binding sites in H44 overlap with translation initiation factor eIF1 (Lomakin *et al*, 2003; Passmore *et al*, 2007), whereas binding of Tsr1 and Dim1 to H28 would interfere with association of the initiator tRNA (Dong *et al*, 2008). Thus, Tsr1 and Dim1 are likely to prevent pre-40S complexes from participating in translation. In addition, the Tsr1- and Dim1-binding sites enclose the 3′ end of the 18S rRNA (Figure 3E), suggesting that their association would impede access of the Nob1 endonuclease to site D (see below).

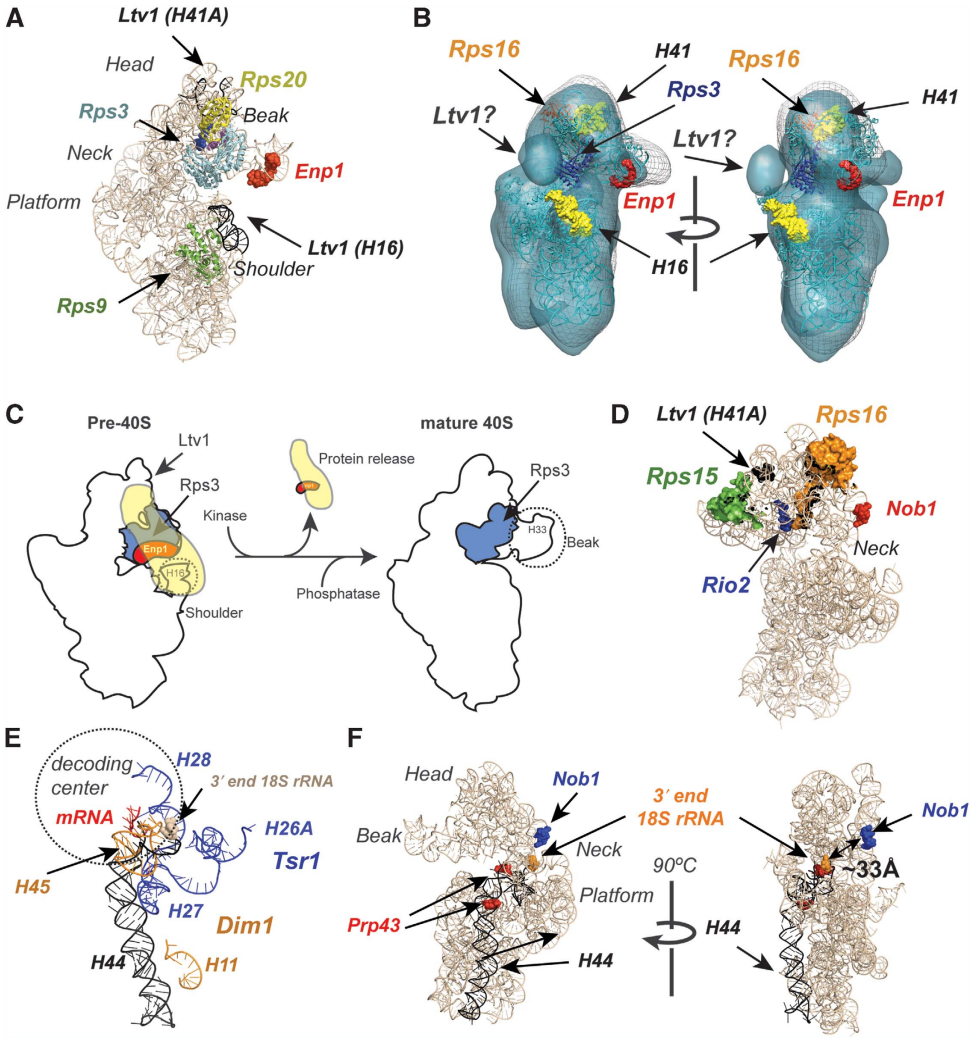

Figure 3 Modelling of protein–RNA interaction sites into 3D structures. (**A**) Modelling of protein–RNA-binding sites in the 40S structure model (pdb 1s1h; Spahn *et al*, 2001). Shown is the model structure of the 18S rRNA. Characteristic structural features are indicated as head, beak, neck, shoulder and platform. Enp1- and Ltv1-binding sites are located near the beak formed by H33. Shown in wheat colour is the 18S rRNA tertiary structure superimposed with ribbon structure models for Rps3 (light blue), Rps9 (green) and Rps20 (yellow). H16 and H41A that interact with Ltv1 are shown in black. Enp1 cross-linking sites in H33 are depicted as red dots. (**B**) Ltv1 may correspond to the extra density near the head and the shoulder in the head domain. The docked molecular model of the yeast 40S subunit is shown for the 40S cryo-EM map (cage) superimposed on the pre-40S cryo-EM map (transparent blue). Helices 16 and 41 surfaces (Ltv1-binding sites) are indicated in yellow, Enp1-binding site surface is indicated in red, Rps3 is indicated in blue and Rps16 is indicated in orange. (**C**) Model for beak formation in pre-40S complexes. On the schematic representation of pre-40S cryo-EM reconstruction images (Schafer *et al*, 2006) the predicted location of Rps3 is indicated in blue. In the model, Hrr25-dependent phosphorylation of Rps3 and subsequent dephosphorylation trigger a structural change leading to repositioning of Rps3, releasing of Enp1 and Ltv1 and beak formation (Schafer *et al*, 2006). Included are the predicted locations of Ltv1 (spanning the head and shoulder domain) and Enp1 (in the centre next to Rps3) in the pre-40S pre-ribosome. (**D**) Rio2, Ltv1 and Nob1-binding sites cluster around Rps16. The surface density of Rps15 and Rps16 in the head domain of the small subunit is shown in green and orange, respectively. The cross-linking sites for Ltv1 (black), Nob1 (red) and Rio2 (blue) are indicated as dots. (**E**) Tsr1 and Dim1 interact with rRNA near the decoding centre. The Tsr1- and Dim1-binding sites were modelled in the *T. thermophilus* 30S crystal structure with bound mRNA (PDB 2wgd) (Voorhees *et al*, 2009). Shown are helices 44, 45 and the RNA segments containing the Tsr1- and Dim1-binding sites (helices 11,26,27,28). The decoding centre is roughly marked with a dashed circle. (**F**) Nob1 binds the head domain in close proximity to the 3′ end of the 18S rRNA. Shown is the tertiary structure model of the 18S rRNA. Nob1 and Prp43 cross-linking sites are indicated as coloured dots. Helix 44 is indicated in black. The arrows indicate the distance (33 Å) between the Nob1 cross-linking site and the modelled 3′-end of the 18S rRNA.

The region surrounding cleavage site D is flexible and not stably associated with Nob1 in pre-40S ribosomes

Nob1 is a PIN-domain endonuclease that cleaves site D at the 3′ end of mature 18S rRNA *in vivo* and *in vitro* (Fatica *et al*, 2003; Pertschy *et al*, 2009). Unusually for a nuclease, Nob1 is stably associated with its substrate. Nob1 interacts with early pre-ribosomal complexes (90S pre-ribosomes) in the nucleolus but remains associated with the pre-40S particles during their export to the cytoplasm, where site D cleavage takes place. This raises the question of what prevents premature, nuclear pre-rRNA cleavage by Nob1?

In CRAC analyses, the most frequent site of Nob1 cross-linking was not at site D, but over helix 40 in the head domain, over 300 nt upstream (Figures 2B and 3F). Of these sequences, 84% contained micro deletions in the terminal loop of H40, precisely identifying the cross-linked nucleotides (Figure 2B, nt 1396–1398). In addition, a few sequences were mapped to H28 (Figure 1A). This indicates that Nob1

primarily binds over the loop of H40, with only transient interactions at cleavage site D.

The PIN domain is characterized by three Asp residues that coordinate a divalent metal ion. Previous analyses showed that mutation of one of these, $D_{15}N$ inhibits site D cleavage *in vivo* and *in vitro* (Fatica *et al*, 2003; Pertschy *et al*, 2009). This mutation does not disrupt Nob1 binding to the 20S pre-rRNA *in vivo* and CRAC analysis on HTP-Nob1 $D_{15}N$ showed that the active site mutation did not dramatically affect association with the 20S pre-rRNA or cross-linking to H40 *in vivo* (Supplementary Figure 4B and C), indicating that the nuclease activity is not required for binding to H40. The HTP-Nob1 $D_{15}N$ mutant is dominant negative and causes accumulation of 20S pre-rRNA (Supplementary Figure 4C), presumably because the mutant protein binds to pre-ribosomes but does not catalyse cleavage. However, the $D_{15}N$ mutant also failed to show significant cross-linking at the D-site region (Supplementary Figure 4B).

Nob1-directed cleavage at site D is a late step in subunit maturation, so the structure of the cytoplasmic pre-40S particle is probably close to the final conformation. In the 3D model of the *Saccharomyces cerevisiae* 40S subunit (Spahn *et al*, 2001), the Nob1 cross-linking site lies ~33 Å away from the 3′ end of the 18S rRNA, equivalent to a stretch of about 10 nucleotides (Figure 3F). However, the model structure lacks the last 8 nt of 18S rRNA, so the actual distance to site D may be less. The dimensions of the dimer of the hSmg6 PIN domain are 36–71–181 Å (Glavan *et al*, 2006). Nob1 is predicted to have similar dimensions and was reported to bind RNA *in vitro* as a tetramer (Lamanna and Karbstein, 2009). We therefore predict that Nob1 bound to H40 could simultaneously interact with site D.

The CRAC data indicated that the majority of pre-40S ribosomes do not have Nob1 bound at site D. To confirm that this does not simply reflect inefficient cross-linking because of RNA structure or other features, dimethyl sulfate (DMS) chemical foot-printing experiments were performed *in vivo* on total pre-ribosomes and *in vitro* on pre-40S complexes (Figure 4). DMS methylates adenines in single stranded or flexible RNA unbound by proteins. The pre-40S particles were purified by precipitation of plasmid expressed HTP-tagged Nob1, which substantially enriched for 20S pre-rRNA (Supplementary Figure 4C).

Primer extension analysis of pre-ribosomes modified with DMS *in vitro* (Figure 4B, lane 4) or *in vivo* (Figure 4C) revealed an almost identical pattern of primer extension stops in the region containing the D cleavage site. The high degree of methylation in the D-site stem indicates that this region is flexible, consistent with previous results (Lamanna and Karbstein, 2009). In contrast, most adenosines in helix 45 and domain I were largely protected from chemical modification, consistent with a stem structure. The DMS probing results were confirmed by *in vitro* modification of the 20S rRNA in purified pre-40S complexes with 1-methyl-7-nitroisatoic anhydride (1M7; Figure 4B, lane 2), which modified 2′-OH residues in single-stranded or flexible regions (Mortimer and Weeks, 2007), and 1-cyclohexyl-(2-morpholinoethyl)carbodiimide metho-p-toluene sulfonate (CMCT) (Figure 4B, lane 3), which modifies unpaired uridines not bound by proteins. Collectively, the cleavages observed are consistent with a largely open structure and indicate that, at least in a subset of particles, Nob1 does not contact the D-site region in purified pre-40S complexes. To substantiate these results we probed the D-site region in Nob1-depleted cells. A glucose repressible Nob1 strain (GAL-3HA::*nob1*) was grown to exponential phase, shifted to glucose containing medium and grown for 8 h at 30°C. Nob1 protein levels were significantly reduced after 8 h in glucose containing medium (Figure 4D) and a substantial accumulation of 20S was detected in these cells (Figure 4E). To quantify the chemical probing data (Figure 4C), signal intensities for each band were normalized to remove differences between lanes. This revealed no significant changes in the intensity or pattern of modifications near the D-site region in Nob1-depleted cells (Figure 4F). We conclude that in pre-40S pre-ribosomes, site D region is very flexible and at steady-state Nob1 is likely not stably associated with the D-cleavage site. The region containing the D-site is normally drawn as a stem structure (Yeh *et al*, 1990) (Figure 4A); however, these data and recent *in vitro* and *in vivo* analyses (Lamanna and Karbstein, 2009) do not support this stem structure.

These observations suggest that alterations in pre-ribosome structure facilitate site D cleavage. Release of Tsr1 and Dim1 may be required for access of Nob1 to the 3′ minor domain. Alternatively, the conformational change in the head domain might bring Nob1 into the correct position for cleavage at site D, and these possibilities are by no means mutually exclusive.

Discussion

Here, we have presented a protein–RNA interaction map for the late pre-40S ribosomes, providing insights into their architecture and maturation. Importantly, we found a good correlation between the CRAC data and previous protein–protein interaction and biochemical data, underlying the reliability of the method. We can now significantly extend the interaction maps as shown in Figure 5.

No crystal structures are available for eukaryotic ribosomes, and the best available structure model for the yeast ribosome was generated using cryo-EM reconstructions and homology modelling (Spahn *et al*, 2001). To relate the binding sites identified in the primary sequence to the 3D structure, we first identified the corresponding sequence in the archaeal rRNA and its position in the crystal structure, which was used to locate the binding site in the yeast structure model. A striking finding was that cross-linking sites for five of the late-acting 40S synthesis factors Rio2, Tsr1, Dim1, Nob1 (this work) and Prp43 (Bohnsack *et al*, 2009) are located in close proximity to functionally important sequence elements in the 3′ region of the 18S rRNA. Intriguingly, the rRNA-binding sites appear to be located in proximity to ribosomal proteins previously shown to be required for D-site cleavage and/or efficient nuclear export of the pre-40S complex (Rps2, Rps3, Rps15 and Rps20, Rps0 and the C-terminus of Rps14) (Tabb-Massey *et al*, 2003; Jakovljevic *et al*, 2004; Leger-Silvestre *et al*, 2004; Ferreira-Cerca *et al*, 2005). This could reflect a general mechanism by which assembly factors prevent stable binding of ribosomal proteins before rRNA maturation steps are completed, as has been proposed for the association of Enp1 and Ltv1 with Rps3.

Notably, the binding sites identified predominately lie in the mature 18S rRNA region, rather than in the transcribed spacers, and are far more common over evolutionarily

conserved regions than over the eukaryotic-specific insertion elements.

In *Escherichia coli*, the emphasis in research into ribosome synthesis has been on the analysis of *in vitro* reconstitution rather than *in vivo* assembly. However, binding sites have been characterized for some factors. The RNA-binding sites for the bacterial orthologue of Dim1 (KsgA) bound to the 30S ribosomal subunit were determined by *in vitro* directed hydroxyl radical cleavage and footprinting experiments (Xu *et al*, 2008). In *E. coli*, KsgA contacts rRNA regions in the 30S subunit that surrounds the modification sites in H45 including H11, 24, 27, 28 and 44 (Supplementary Figure 5) and these interactions are proposed to be important in preventing premature interactions of pre-30S particles with

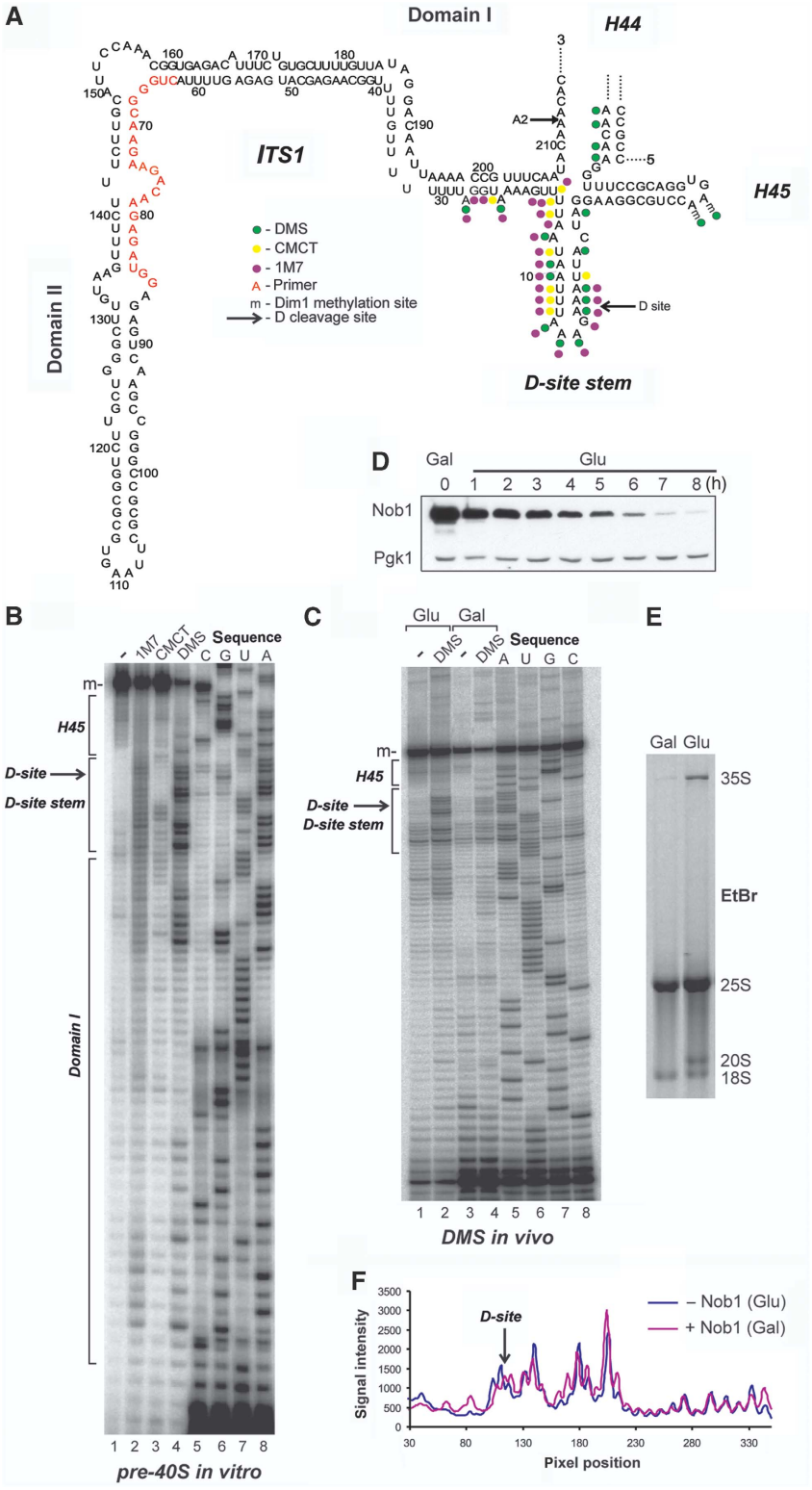

the translation machinery. Yeast Dim1 can complement an *E. coli ksgA*Δ mutant (Lafontaine *et al*, 1994) and Dim1 cross-linking sites on the 18S rRNA included analogous positions (Supplementary Figure 5). We conclude that both the methyl transferase function of Dim1 and its interactions with the rRNA are conserved in evolution.

Ribosome biogenesis in bacteria involves several different GTPases, which are proposed to act as 'molecular switches', regulating the stepwise assembly and maturation of RNA–protein subcomplexes (reviewed in Culver, 2001; Karbstein, 2007; Connolly and Culver, 2009). Two bacterial GTPases required for 16S rRNA processing (Era and RsgA/YjeQ) are genetically linked to KgsA (Inoue *et al*, 2006; Campbell and Brown, 2008). Cryo-EM microscopy studies revealed that some sites of Era interaction with the 16S rRNA are at positions analogous to the Tsr1-binding sites in yeast (H26, H28, H44, H45) (Sharma *et al*, 2005). Similarly, RsgA also contacts the 3′ minor domain and GTP-bound RsgA causes structural rearrangements in H44 (Kimura *et al*, 2008). The overlap in RNA-binding sites observed for Dim1 and Tsr1 strongly suggest that they interact directly in pre-40S complexes. We predict that Tsr1 and Dim1 together fulfill functions in ribosome assembly that are equivalent to KsgA and Era/RsgA in bacteria.

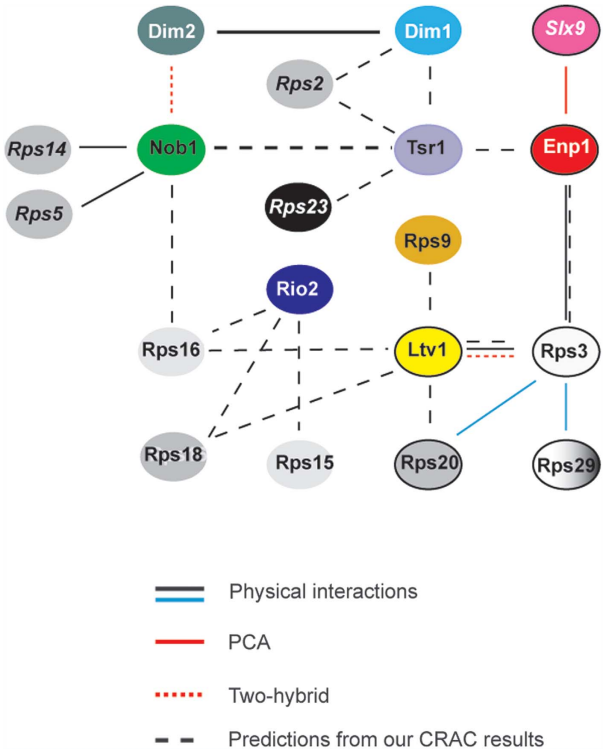

Figure 5 Overview of known and predicted protein–protein interactions in pre-40S complexes. The interaction map depicts interactions between the various assembly factors and ribosomal proteins in pre-40S complexes. Black lines, physical interactions among proteins shown to be part of subcomplexes or interacting as recombinant proteins (Krogan *et al*, 2004; Vanrobays *et al*, 2004; Schafer *et al*, 2006; Tarassov *et al*, 2008; Lamanna and Karbstein, 2009). Dashed red lines, yeast two-hybrid interactions (Ito *et al*, 2001; Tone and Toh, 2002). Red lines, interactions from protein–fragment complementation assays (PCA), which detect proteins within 80 Å distance from each other (Tarassov *et al*, 2008). Dashed black lines, protein–protein interactions predicted from our CRAC data. Blue lines, physical interactions among bacterial homologues of the indicated proteins (Brodersen *et al*, 2002).

The Rio2 protein kinase is required for 20S–18S processing, but its targets are unknown. In the 40S structure model, the Rio2-binding site is located close to Rps15, (Figure 3D) and pre-40S ribosomes that lack Rps15 fail to efficiently incorporate Rio2 and are not efficiently exported to the cytoplasm (Leger-Silvestre *et al*, 2004; Zemp *et al*, 2009). This suggests that these proteins interact directly. Human Rio2 kinase activity is required for release of hNob1, hLtv1 and hDim2 from pre-40S ribosomes (Zemp *et al*, 2009) and the binding sites for yeast Rio2, Ltv1 and Nob1 are closely located in the head domain. These sites are also close to Rps16 and Rps18 (Figure 3D). The bacterial Rps18 homologue (S13) is phosphorylated at serine and threonine residues (Soung *et al*, 2009) and this may also be the case for bacterial Rps16 (S9) (Traugh and Traut, 1972), suggesting Rps16 and Rps18 as potential Rio2 substrates.

Pre-40S particles lack the prominent beak structure present in the mature subunit, implying large-scale structural reorganization during 40S maturation (Schafer *et al*, 2006). Two 40S synthesis factors, Enp1 and Ltv1, were implicated in this reorganization but their actual roles were unclear. We report that Enp1 directly binds sequences in H33 that will form the beak. Ltv1 binds sequences in H41, which are located close to the beak, but also binds H16, which is more distantly located in the shoulder region of the 40S particle. If Ltv1 binds both sequences simultaneously, it would need to span the head–shoulder gap—a distance of some 87 Å in the mature 40S subunit. Ltv1 is ∼53 kDa and, assuming a monomer with cylindrical shape and an average density of 0.73 cm^3/g, an 87 Å long Ltv1 protein would have a diameter of ∼30 Å. Comparison of the cryo-EM maps for pre-40S and mature 40S

Figure 4 At steady state the stem structure containing the D-cleavage site is highly flexible and unbound by proteins. (**A**) Overview of the chemical foot-printing results on a secondary structure of ITS1, including the 5′ end of the 18S rRNA, adopted from Yeh *et al* (1990). Red nucleotides indicate the location of the reverse transcriptase primer. Adenosines in H45 dimethylated by Dim1 *in vivo* are indicated with '-m'. Green circles indicate the nucleotide modified by DMS. Yellow and purple dots indicate the CMCT and 1M7-modified nucleotides, respectively. (**B**) The D-site region in purified 20S pre-rRNA is flexible and unbound by proteins. DMS, CMCT and 1M7 modification of RNA was performed at 30°C on purified pre-40S complexes isolated using plasmid-expressed HTP-tagged Nob1 as bait. All chemicals primarily modified nucleotides in the D-site stem region, indicating it is flexible or single stranded, whereas other regions predicted to be double stranded (i.e. H45 and Domain I) were largely protected from chemical modification. Adenosines in H45 dimethylated by Dim1 *in vivo* are indicated with '-m'. (**C**–**F**) The D-site helix is highly flexible and likely unbound by Nob1 *in vivo*. *In vivo* DMS was performed at 30°C on total RNA purified from GAL::3HA-nob1 cells (**E**) grown in glucose for 8 h (**C**, lanes 1 and 2) or galactose (**C**, lanes 3 and 4). Depletion of Nob1 was confirmed by western blotting (**D**) using an HRP-conjugated anti-HA antibody (Santa Cruz) and accumulation of 20S pre-rRNA was detected by ethidium bromide staining of total RNA in an agarose gel. Pgk1 antibodies (Santa Cruz) were used to confirm loading of equal amounts proteins on each lane (**D**). After primer extension, radiolabelled cDNAs were resolved on 12% polyacrylamide/7 M urea gels and visualized by autoradiography. Adenosines in H45 dimethylated by Dim1 *in vivo* are indicated with '-m'. Quantification of chemical probing data (**F**) was performed as described in the main text.

revealed extra density the side of the head domain in pre-40S particles, close to the location predicted for Ltv1 (Figure 3B) (Schafer *et al*, 2006). The volume of this region would be in good agreement with the presence of a protein of ~53 kDa (B Böttcher, personal communication).

To better facilitate the interpretation of the cryo-EM images, we manually docked the 40S structure model (1s1h) (Spahn *et al*, 2001) onto the 40S cryo-EM map (mesh model in Figure 3B) (Schafer *et al*, 2006) and overlaid this with the pre-40S cryo-EM map (transparent blue). This provided a reasonable estimation of location of ribosomal proteins and RNA structures in pre-40S pre-ribosomes. In the pre-40S EM map, the shoulder formed by H16 is absent or poorly defined, however, the extra density appears to be located parallel to Rps3 and just above H16. We therefore predict that this density corresponds to Ltv1, although we cannot exclude the possibility that multiple copies of Ltv1 are present.

The CRAC data revealed that Dim1, Tsr1 and Rio2 bind 18S rRNA regions that are important for the association of translation factors, tRNAs and 60S subunit joining. In the case of Dim1 and Tsr1, these are conserved to *E. coli* and in both bacterial and eukaryotic ribosomes are incompatible with binding to the mRNA, 60S subunit, initiator tRNA and translation factors. Dissociation of each of these proteins from the pre-40S particles would therefore be required for translation to commence. Pre-40S complexes were recently reported to associate with polysomes (Soudet *et al*, 2010), particularly after depletion of Nob1 or the Rio1 kinase. These conditions prevent 18S maturation, resulting in a very substantial 20S pre-rRNA accumulation, which is readily visible by ethidium bromide staining of total RNA. We predict that not all of this large pool of accumulated pre-40S particles can be associated with the ribosome synthesis factors, and their absence may explain the ability of the defective pre-40S ribosomes to engage with the translation machinery (Soudet *et al*, 2010).

Nob1 is the PIN-domain endonuclease that cleaves site D at the 3′ end of 18S rRNA (Fatica *et al*, 2003; Pertschy *et al*, 2009). Unexpectedly, the major binding site identified for Nob1 was located in H40, distinct from the cleavage site. Binding to and cleavage of site D requires the PIN domain (Fatica *et al*, 2004; Lamanna and Karbstein, 2009; Pertschy *et al*, 2009). This indicates that H40 recognition involves a different region of Nob1, most likely the C-terminal, Zn-ribbon putative RNA-binding domain, potentially leaving the PIN domain free to recognize the cleavage site.

Nob1 associates with 90S pre-ribosome early in 40S subunit synthesis pathway, but cleaves site D only in very late pre-40S particles after nuclear export (Fatica *et al*, 2003; Pertschy *et al*, 2009). Structure probing revealed that the region containing the D-cleavage site is readily accessible to chemical modification within pre-ribosomes, both *in vitro* and *in vivo*. This indicates that it is largely unstructured and unbound by proteins, and should therefore be accessible to the nuclease. What then prevents Nob1 from cleaving site D in early pre-ribosomes? The pre-40S cross-linking data reported here and by Bohnsack *et al* (2009) identified four putative enzymes interacting with the decoding centre and with H44 (Tsr1, Rio2, Dim1 and Prp43), strongly implying that this region undergoes restructuring; as does the homologous region in bacteria. Notably, Dim1 also binds early, nuclear pre-ribosomes, but methylates the 3′ end of 18S rRNA much later in the pathway, after export to the cytoplasm. Restructuring might not only be essential for the correct folding of the 3′ domain of the 18S rRNA, but also to allow cleavage at site D to occur. On the basis of 3D modelling, we speculate that only when the structure of 3′ domain of 18S is close to its final conformation, can Nob1 access and cleave site D. In 3D models, the Tsr1- and Dim1-binding sites are in close proximity to the 3′ end of the 18S rRNA in the pre-40S and it is conceivable that both proteins could interfere with D-site cleavage by sterically hindering Nob1 binding to the cleavage site. We therefore predict that both RNA restructuring and protein remodelling steps in the 3′ region of the 18S rRNA are necessary for Nob1-dependent cleavage at site D.

Cryo-EM studies showed that binding of yeast translation initiation factors eIF1-eIF1A to the small subunit induces a conformational change that leads to a connection between the head and the shoulder, mediated by Rps3 and H16 (Passmore *et al*, 2007). This interaction stabilizes the head domain and prevents the 'mRNA latch' from forming prematurely, making the mRNA-binding channel more accessible to the large cap-binding protein complex attached to the 5′ end of the mRNA (Passmore *et al*, 2007). We propose that Ltv1 binding to both Rps3 and H16 locks the head into the pre-ribosome conformation, whereas Enp1 binding to Rps3 and H33 directly prevents formation of the beak structure (Figure 3C). The 40S subunit is characterized by structural changes during the translation cycle, and it appears that large-scale structural changes also feature it its maturation.

Materials and methods

Yeast strains and media

S. cerevisiae strain BY4741 (MATa; *his3Δ1; leu2Δ0; met15Δ0; ura3Δ0*) was used as the parental strain (Brachmann *et al*, 1998). The HTP carboxyl-tagged strains (Supplementary Table 3) were generated by PCR as described (Rigaut *et al*, 1999) using oligonucleotides listed in Supplmentary Table 2. Strains were grown in YPD (1% yeast extract, 2% peptone, 2% dextrose) or YPG/R (YP with 2% galactose and 2% raffinose) at 30°C.

Cross-linking and analyses of cDNA (CRAC)

In vivo CRAC, western and northern blot analyses were performed as described earlier (Granneman *et al*, 2009) with the following modifications: for the Ltv1 and Tsr1 CRAC experiments TEV eluates were incubated with lower amounts of RNase (0.1–0.5 units of RNaceIT (Stratagene), depending on the batch used) for 5 min at 37°C. For cloning the 5′ Solexa and miRCat-33 linkers were used (Integrated DNA technologies, UK) (Granneman *et al*, 2009).

Sequence analysis

Sanger sequencing of cDNAs was performed as described (Granneman *et al*, 2009). Sequences were analysed with Blast (http://blast.ncbi.nlm.nih.gov). The sequences (inserts) located between pairs of linkers were extracted and analysed for homology with yeast RNAs. The choice of blast parameters did not qualitatively affect the results; we typically used word size, 8; expectation value, 0.1; other parameters were set to default. We then computed, for each position along the sequence of interest, the number of inserts covering that position. The Blast output was used to generate histograms shown in Figure 1 and Supplementary Figure 3. To map the substitutions and deletions and generate sequence alignments, fasta files containing the insert were aligned to the rDNA reference sequence using Novoalign 2.04 (http://www.novocraft.com) as described earlier (Granneman *et al*, 2009). The Novoalign output was used to generate the multiple sequence alignments shown in Supplementary data online. A set of Awk and Perl scripts for automated sequence analysis in Windows, Mac or Linux environments is available on request.

Immunoprecipitation experiments

Cells were grown in 50 ml of YPD to an OD600 of 0.5, collected and washed with phosphate-buffered saline. Extracts were prepared in 500 µl of Buffer A (50 mM Tris pH 7.5, 1.5 mM $MgCl_2$, 150 mM NaCl, 0.1% NP-40, 5 mM β-mercaptoethanol and protease inhibitors (Roche)) using Zirconia beads as described earlier (Granneman *et al*, 2009). RNA extractions and northern blot analyses were performed as described earlier (Tollervey, 1987) using oligonucleotides listed in Supplementary Table 2. Supplementary Figure 1 shows the regions to which the oligonucleotides hybridize.

In vitro chemical modification of purified pre-40S complexes

One litre of BY4741 cells containing the pADH-HTP-Nob1 plasmid (a generous gift from Brigitte Pertschy) was grown to an OD600 of 0.5. Extracts were prepared in 4 ml of Buffer B (50 mM Hepes–KOH pH 7.5, 100 mM NaAc, 5 mM $MgCl_2$, 5 mM β-mercaptoethanol, 0.1% NP-40 and protease inhibitors (Roche)). For each purification, 1 ml of extract was incubated with 50 µl of IgG beads for 1 h at 4°C. IgG beads were washed three times with Buffer B and resuspended in 50 µl of Buffer B for chemical modification reactions. DMS modification was performed in Buffer B for 10 min at 30°C using 10 µl of 20% DMS (diluted into ethanol). The reaction was quenched by addition of 40 µl of mix 0.5 M β-mercaptoethanol and 0.5 M sodium acetate pH 5.5. One-methyl-7-nitroisatoic anhydride (1M7; Fisher Scientific) modification reactions were performed in Buffer A at 30°C for 1 min in the presence of 8 mM 1M7. CMCT modification reactions were performed in Buffer C (50 sodium borate pH 7.5, 100 KCl, 5 mM $MgCl_2$), for 10 min at 30°C using 30 µl of 80 mg/ml CMCT, freshly prepared in water. To map the modified nucleotides, primer extension reactions were performed using oligonucleotide ITS1 RT (Supplementary Table 2) as described earlier (Granneman *et al*, 2009) using ~100 ng of purified RNA or 1 µg of total RNA. CDNAs were resolved on 12%/7 M urea gels and visualized by autoradiography.

In vivo structural probing with DMS was performed essentially as described earlier (Ares and Igel, 1990). The YAF34 strain (Gal::3HA-nob1 ;(Fatica *et al*, 2003) was grown in YPG/R to logarithmic phase, shifted to YPD and then grown for 8 h at 30°C. Subsequently, 10 ml of cells was incubated at 30°C for 2 min with 200 µl of 33% DMS (diluted in ethanol). The reaction was quenched by addition of 5 ml 0.7 M β-mercaptoethanol and 5 ml water-saturated isoamyl-alcohol. Modified nucleotides were identified by primer extension as described above. Quantification of chemical modification reactions was performed using the Fuji-FLA-5100 phospho-imager scanner and the AIDA software package according to the manufacturers procedures.

Modelling of RNA-binding sites

To visualize the RNA-binding sites in the *S. cerevisiae* 3D model structure (Spahn *et al*, 2001) or the *T. thermophilus* 70S crystal structure (Voorhees *et al*, 2009), we determined corresponding regions in the *T. thermophilus* 16S rRNA and *Haloarcula marismortui* 23S rRNA. Using Pymol we then visualized the locations in the model structures (PDBs 1s1h, 1s1i and 2wdg). We used chimaera (http://www.cgl.ucsf.edu/chimera/) (Goddard *et al*, 2007) to manually dock the 40S model structure (Spahn *et al*, 2001) in cryo-EM reconstructions (emd_1211 and end_1212) according to the chimaera documentation.

Supplementary data

Supplementary data are available at *The EMBO Journal* Online (http://www.embojournal.org).

Acknowledgements

We thank Grzegorz Kudla for bioinformatics support and help with 4F, Bettina Böttcher for help with interpretation of cryo-EM images, Zhili Xu and Gloria Culver for providing the KsgA footprinting data figure, Simon Lebaron and Claudia Schneider for communicating unpublished results, Brigitte Pertschy for the pADH-HTP-Nob1 construct, the Edinburgh Gene Pool Sequencing Facility and the Swann Building kitchen staff. SG and DT designed the research. SG, EP and AG performed the research and analysed the data. SG and DT wrote the paper. This work was supported by the Welcome Trust, the BBSRC (BB/D019621/1), EMBO long-term fellowship (SG) and a Marie Curie EIF fellowship (SG).

Conflict of interest

The authors declare that they have no conflict of interest.

References

Antunez de Mayolo P, Woolford JL, Jr. (2003) Interactions of yeast ribosomal protein rpS14 with RNA. *J Mol Biol* **133:** 697–709

Ares Jr M, Igel AH (1990) Lethal and temperature-sensitive mutations and their suppressors identify an essential structural element in U2 small nuclear RNA. *Genes Dev* **4:** 2132–2145

Bohnsack MT, Martin R, Granneman S, Ruprecht M, Schleiff E, Tollervey D (2009) Prp43 bound at different sites on the pre-rRNA performs distinct functions in ribosome synthesis. *Mol Cell* **36:** 583–592

Brodersen DE, Clemons Jr WM, Carter AP, Wimberly BT, Ramakrishnan V (2002) Crystal structure of the 30 S ribosomal subunit from Thermus thermophilus: structure of the proteins and their interactions with 16 S RNA. *J Mol Biol* **316:** 725–768

Brachmann CB, Davies A, Cost GJ, Caputo E, Li J, Hieter P, Boeke JD (1998) Designer deletion strains derived from Saccharomyces cerevisiae S288C: a useful set of strains and plasmids for PCR-mediated gene disruption and other applications. *Yeast* **14:** 115–132

Campbell TL, Brown ED (2008) Genetic interaction screens with ordered overexpression and deletion clone sets implicate the Escherichia coli GTPase YjeQ in late ribosome biogenesis. *J Bacteriol* **190:** 2537–2545

Clemons Jr WM., May JL, Wimberly BT, McCutcheon JP, Capel MS, Ramakrishnan V (1999) Structure of a bacterial 30S ribosomal subunit at 5.5 A resolution. *Nature* **400:** 833–840

Connolly K, Culver G (2009) Deconstructing ribosome construction. *Trends Biochem Sci* **34:** 256–263

Culver GM (2001) Meanderings of the mRNA through the ribosome. *Structure* **9:** 751–758

Dong J, Nanda JS, Rahman H, Pruitt MR, Shin BS, Wong CM, Lorsch JR, Hinnebusch AG (2008) Genetic identification of yeast 18S rRNA residues required for efficient recruitment of initiator tRNA(Met) and AUG selection. *Genes Dev* **22:** 2242–2255

Dresios J, Chan YL, Wool IG (2005) A determination of the identity elements in yeast 18 S ribosomal RNA for the recognition of ribosomal protein YS11: the role of the kink-turn motif in helix 11. *J Mol Biol* **345:** 681–693

Fatica A, Oeffinger M, Dlakic M, Tollervey D (2003) Nob1p is required for cleavage of the 3′ end of 18S rRNA. *Mol Cell Biol* **23:** 1798–1807

Fatica A, Tollervey D, Dlakic M (2004) PIN domain of Nob1p is required for D-site cleavage in 20S pre-rRNA. *RNA* **10:** 1431–1436

Ferreira-Cerca S, Poll G, Gleizes PE, Tschochner H, Milkereit P (2005) Roles of eukaryotic ribosomal proteins in maturation and transport of pre-18S rRNA and ribosome function. *Mol Cell* **20:** 263–275

Fromont-Racine M, Senger B, Saveanu C, Fasiolo F (2003) Ribosome assembly in eukaryotes. *Gene* **313:** 17–42

Gelperin D, Horton L, Beckman J, Hensold J, Lemmon SK (2001) Bms1p, a novel GTP-binding protein, and the related Tsr1p are required for distinct steps of 40S ribosome biogenesis in yeast. *RNA* **7:** 1268–1283

Glavan F, Behm-Ansmant I, Izaurralde E, Conti E (2006) Structures of the PIN domains of SMG6 and SMG5 reveal a nuclease within the mRNA surveillance complex. *EMBO J* **25:** 5117–5125

Goddard TD, Huang CC, Ferrin TE (2007) Visualizing density maps with UCSF Chimera. *J Struct Biol* **157:** 281–287

Granneman S, Kudla G, Petfalski E, Tollervey D (2009) Identification of protein binding sites on U3 snoRNA and pre-rRNA by UV cross-linking and high-throughput analysis of cDNAs. *Proc Natl Acad Sci USA* **106:** 9613–9618

Henras AK, Soudet J, Gerus M, Lebaron S, Caizergues-Ferrer M, Mougin A, Henry Y (2008) The post-transcriptional steps of eukaryotic ribosome biogenesis. *Cell Mol Life Sci* **65:** 2334–2359

Inoue K, Chen J, Tan Q, Inouye M (2006) Era and RbfA have overlapping function in ribosome biogenesis in Escherichia coli. *J Mol Microbiol Biotechnol* **11:** 41–52

Ito T, Chiba T, Ozawa R, Yoshida M, Hattori M, Sakaki Y (2001) A comprehensive two-hybrid analysis to explore the yeast protein interactome. *Proc Natl Acad Sci USA* **98:** 4569–4574

Jakovljevic J, Antunez de Mayolo P, Miles TD, Nguyen TML, Leger-Silvestre I, Gas N, Woolford Jr JL. (2004) The Carboxy-terminal extension of yeast ribosomal protein S14 is necessary for maturation of 43S pre-ribosomes. *Mol Cell* **14:** 331–342

Karbstein K (2007) Role of GTPases in ribosome assembly. *Biopolymers* **87:** 1–11

Kimura T, Takagi K, Hirata Y, Hase Y, Muto A, Himeno H (2008) Ribosome-small-subunit-dependent GTPase interacts with tRNA-binding sites on the ribosome. *J Mol Biol* **381:** 467–477

Krogan NJ, Peng WT, Cagney G, Robinson MD, Haw R, Zhong G, Guo X, Zhang X, Canadien V, Richards DP, Beattie BK, Lalev A, Zhang W, Davierwala AP, Mnaimneh S, Starostine A, Tikuisis AP, Grigull J, Datta N, Bray JE *et al* (2004) High-definition macromolecular composition of yeast RNA-processing complexes. *Mol Cell* **13:** 225–239

Lafontaine D, Delcour J, Glasser AL, Desgres J, Vandenhaute J (1994) The DIM1 gene responsible for the conserved m6(2)Am6(2)A dimethylation in the 3′-terminal loop of 18 S rRNA is essential in yeast. *J Mol Biol* **241:** 492–497

Lafontaine D, Vandenhaute J, Tollervey D (1995) The 18S rRNA dimethylase Dim1p is required for pre-ribosomal RNA processing in yeast. *Genes Dev* **9:** 2470–2481

Lamanna AC, Karbstein K (2009) Nob1 binds the single-stranded cleavage site D at the 3′-end of 18S rRNA with its PIN domain. *Proc Natl Acad Sci USA* **106:** 14259–14264

Leger-Silvestre I, Milkereit P, Ferreira-Cerca S, Saveanu C, Rousselle JC, Choesmel V, Guinefoleau C, Gas N, Gleizes PE (2004) The ribosomal protein Rps15p is required for nuclear exit of the 40S subunit precursors in yeast. *EMBO J* **23:** 2336–2347

Liang XH, Liu Q, Fournier MJ (2009) Loss of rRNA modifications in the decoding center of the ribosome impairs translation and strongly delays pre-rRNA processing. *RNA* **15:** 1716–1728

Lomakin IB, Kolupaeva VG, Marintchev A, Wagner G, Pestova TV (2003) Position of eukaryotic initiation factor eIF1 on the 40S ribosomal subunit determined by directed hydroxyl radical probing. *Genes Dev* **17:** 2786–2797

Mortimer SA, Weeks KM (2007) A fast-acting reagent for accurate analysis of RNA secondary and tertiary structure by SHAPE chemistry. *J Am Chem Soc* **129:** 4144–4145

Nissan TA, Galani K, Maco B, Tollervey D, Aebi U, Hurt E (2004) A pre-ribosome with a tadpole-like structure functions in ATP-dependent maturation of 60S subunits. *Mol Cell* **15:** 295–301

Passmore LA, Schmeing TM, Maag D, Applefield DJ, Acker MG, Algire MA, Lorsch JR, Ramakrishnan V (2007) The eukaryotic translation initiation factors eIF1 and eIF1A induce an open conformation of the 40S ribosome. *Mol Cell* **26:** 41–50

Pertschy B, Schneider C, Gnadig M, Schafer T, Tollervey D, Hurt E (2009) RNA helicase Prp43 and its co-factor Pfa1 promote 20 to 18 S rRNA processing catalyzed by the endonuclease Nob1. *J Biol Chem* **284:** 35079–35091

Rigaut G, Shevchenko A, Rutz B, Wilm M, Mann M, Séraphin B (1999) A generic protein purification method for protein complex characterization and proteome exploration. *Nat Biotechnol* **17:** 1030–1032

Schafer T, Maco B, Petfalski E, Tollervey D, Bottcher B, Aebi U, Hurt E (2006) Hrr25-dependent phosphorylation state regulates organization of the pre-40S subunit. *Nature* **441:** 651–655

Schafer T, Strauss D, Petfalski E, Tollervey D, Hurt E (2003) The path from nucleolar 90S to cytoplasmic 40S pre-ribosomes. *EMBO J* **22:** 1370–1380

Seiser RM, Sundberg AE, Wollam BJ, Zobel-Thropp P, Baldwin K, Spector MD, Lycan DE (2006) Ltv1 is required for efficient nuclear export of the ribosomal small subunit in Saccharomyces cerevisiae. *Genetics* **174:** 679–691

Sharma MR, Barat C, Wilson DN, Booth TM, Kawazoe M, Hori-Takemoto C, Shirouzu M, Yokoyama S, Fucini P, Agrawal RK (2005) Interaction of Era with the 30S ribosomal subunit implications for 30S subunit assembly. *Mol Cell* **18:** 319–329

Soudet J, Gelugne JP, Belhabich-Baumas K, Caizergues-Ferrer M, Mougin A (2010) Immature small ribosomal subunits can engage in translation initiation in Saccharomyces cerevisiae. *EMBO J* **29:** 80–92

Soung GY, Miller JL, Koc H, Koc EC (2009) Comprehensive Analysis of Phosphorylated Proteins of Escherichia coli Ribosomes. *J Proteome Res* **8:** 3390–3402

Spahn CM, Beckmann R, Eswar N, Penczek PA, Sali A, Blobel G, Frank J (2001) Structure of the 80S ribosome from Saccharomyces cerevisiae–tRNA-ribosome and subunit-subunit interactions. *Cell* **107:** 373–386

Tabb-Massey A, Caffrey JM, Logsden P, Taylor S, Trent JO, Ellis SR (2003) Ribosomal proteins Rps0 and Rps21 of Saccharomyces cerevisiae have overlapping functions in the maturation of the 3′ end of 18S rRNA. *Nucleic Acids Res* **31:** 6798–6805

Tarassov K, Messier V, Landry CR, Radinovic S, Serna Molina MM, Shames I, Malitskaya Y, Vogel J, Bussey H, Michnick SW (2008) An *in vivo* map of the yeast protein interactome. *Science* **320:** 1465–1470

Tollervey D (1987) A yeast small nuclear RNA is required for normal processing of pre-ribosomal RNA. *EMBO J* **6:** 4169–4175

Tone Y, Toh EA (2002) Nob1p is required for biogenesis of the 26S proteasome and degraded upon its maturation in Saccharomyces cerevisiae. *Genes Dev* **16:** 3142–3157

Traugh JA, Traut RR (1972) Phosphorylation of ribosomal proteins of Escherichia coli by protein kinase from rabbit skeletal muscle. *Biochemistry* **11:** 2503–2509

Ulbrich C, Diepholz M, Bassler J, Kressler D, Pertschy B, Galani K, Bottcher B, Hurt E (2009) Mechanochemical removal of ribosome biogenesis factors from nascent 60S ribosomal subunits. *Cell* **138:** 911–922

Vanrobays E, Gelugne JP, Caizergues-Ferrer M, Lafontaine DL (2004) Dim2p, a KH-domain protein required for small ribosomal subunit synthesis. *RNA* **10:** 645–656

Vanrobays E, Gelugne JP, Gleizes PE, Caizergues-Ferrer M (2003) Late cytoplasmic maturation of the small subunit requires RIO proteins in *Saccharomyces cerevisiae*. *Mol Cell Biol* **23:** 2083–2095

Voorhees RM, Weixlbaumer A, Loakes D, Kelley AC, Ramakrishnan V (2009) Insights into substrate stabilization from snapshots of the peptidyl transferase center of the intact 70S ribosome. *Nat Struct Mol Biol* **16:** 528–533

Xu Z, O'Farrell HC, Rife JP, Culver GM (2008) A conserved rRNA methyltransferase regulates ribosome biogenesis. *Nat Struct Mol Biol* **15:** 534–536

Yeh LC, Thweatt R, Lee JC (1990) Internal transcribed spacer 1 of the yeast precursor ribosomal RNA. Higher order structure and common structural motifs. *Biochemistry* **29:** 5911–5918

Zemp I, Wild T, O'Donohue MF, Wandrey F, Widmann B, Gleizes PE, Kutay U (2009) Distinct cytoplasmic maturation steps of 40S ribosomal subunit precursors require hRio2. *J Cell Biol* **185:** 1167–1180

